

# Conditions for the invertibility of dual energy data

Robert E. Alvarez\*

November 8, 2018

The Alvarez-Macovski method [Alvarez, R. E and Macovski, A., "Energy-selective reconstructions in X-ray computerized tomography", Phys. Med. Biol. (1976), 733–44] requires the inversion of the transformation from the line integrals of the basis set coefficients to measurements with multiple x-ray spectra. Analytical formulas for invertibility of the transformation from two measurements to two line integrals are derived. It is found that non-invertible systems have near zero Jacobian determinants on a nearly straight line in the line integrals plane. Formulas are derived for the points where the line crosses the axes, thus determining the line. Additional formulas are derived for the values of the terms of the Jacobian determinant at the endpoints of the line of non-invertibility. The formulas are applied to a set of spectra including one suggested by Levine that is not invertible as well as similar spectra that are invertible and voltage switched x-ray tube spectra that are also invertible. An iterative inverse transformation algorithm exhibits large errors with non-invertible spectra.

Key Words: spectral x-ray, dual energy, energy selective, inverse

## 1 Introduction

In the Alvarez-Macovski[1] method for extracting x-ray spectral data, the attenuation coefficient is expanded as a linear combination of functions of energy multiplied by basis set coefficients that depend on the composition of the material at points within the object. The line integrals of the basis set coefficients are then computed by inverting the transformation from the measurements with multiple spectra. Summarizing the measurements by the vector  $\mathbf{L}$  and the line integrals of the basis set coefficients as the vector  $\mathbf{A}$ , we need to show that the transformation  $\mathbf{L}(\mathbf{A})$  is invertible. This question is examined in this paper. In particular, the transformation for a noise-free system using two measurement spectra with a two function basis set, *i.e.* a dual energy system, is studied.

Invertibility is of more than mathematical interest since spectra that are near non-invertible can lead to a large multiplication of noise in the output images. In the past, dual energy systems used measurements with two different x-ray tube voltages or a fixed tube voltage and filtering with two materials both with energy integrating detectors. Experience showed that these were invertible. However, the introduction of photon counting detectors into clinical systems[2] leads to potential invertibility problems due to the imperfections in these detectors[3] such as pileup, K-radiation escape, charge sharing, and others. My recent paper[4] showed that a large pileup factor can lead to non-invertibility for a three dimension A-vector with three bin pulse height analysis and that this non-invertibility leads to large increases in noise.

I discussed invertibility in other papers. In early work[5, 6], I showed that a general, two dimensional inversion theorem[7] could be applied to the dual energy transformation. The theorem requires that the transformation be invertible on a closed contour in the first quadrant of the A-vector plane and have a non-zero Jacobian determinant inside the contour. I showed that the transformation is invertible on the contour if the two spectra have different maximum energies. The proof was for ordinary energy integrating detectors as well as photon counting detectors without pileup. Later, I showed that the transformation is invertible on the contour for photon counting detectors with pileup[8].

Recently, Levine[9] described a different approach to determining invertibility. He studied a system with energy spectra with only three discrete energies, no scatter and a perfect detector. He found that, with appropriately chosen spectral values, the transformation is not one-to-one and is therefore not invertible. The spectra had the same maximum energy so my previous results were not applicable.

---

\*aprendtech.com, ralvarez@aprendtech.com

My papers did not address the proof that the Jacobian determinant is non-zero within the contour. In this paper, I derive analytical formulas are derived to test for the non-zero condition for a set of measurement spectra and detector. The formulas are applied to several systems including (1) the set proposed by Levine[9] that are not invertible as well as (2) similar spectra that are invertible and (3) invertible voltage switched x-ray tube spectra that have long been used in dual energy imaging. The results are verified by testing the errors with an iterative algorithm that inverts the transformation.

## 2 Methods

### 2.1 The transformation

This section reviews the Alvarez-Macovski method[1], introduces notation, and specifies the transformation that is required to be inverted for the method.

For biological materials, we can approximate the x-ray attenuation coefficient  $\mu(\mathbf{r}, E)$  with a two function basis set[10]

$$\mu(\mathbf{r}, E) = a_1(\mathbf{r})f_1(E) + a_2(\mathbf{r})f_2(E). \quad (1)$$

In this equation, the coefficients  $a_i(\mathbf{r})$  are functions only of the material composition at a position  $\mathbf{r}$  within the object and the functions  $f_i(E)$  depend only on the x-ray energy  $E$ . If there is a high atomic number contrast agent, we can extend the basis set to higher dimensions.

Neglecting scatter, the expected value of the number of transmitted photons  $\lambda_k$  with an effective measurement spectrum  $S_k(E)$  is

$$\lambda_k = \int S_k(E) e^{-\int_{\mathcal{L}} \mu(\mathbf{r}, E) d\mathbf{r}} dE \quad (2)$$

where the line integral in the exponent is on a line  $\mathcal{L}$  from the x-ray source to the detector. The effective measurement spectra include the effects of the source spectrum and the detector response. Using the attenuation coefficient decomposition, Eq. 1, the line integral is

$$\int_{\mathcal{L}} \mu(\mathbf{r}, E) d\mathbf{r} = A_1 f_1(E) + A_2 f_2(E). \quad (3)$$

where  $A_i = \int_{\mathcal{L}} a_i(\mathbf{r}) d\mathbf{r}$ ,  $i = 1 \dots 2$  are the line integrals of the basis set coefficients. If the  $A_i$  are summarized as the components of the A-vector,  $\mathbf{A}$ , and the basis functions at energy  $E$  by the vector  $\mathbf{f}(\mathbf{E})$ , the expected values in Eq. 2 are

$$\lambda_k(\mathbf{A}) = \int S_k(E) e^{-\mathbf{A} \cdot \mathbf{f}(\mathbf{E})} dE. \quad (4)$$

This paper assumes noise free data so the measurements are the expected values. These measurements are summarized by a vector,  $\mathbf{N}$ , whose components are the expected value of the photon counts with each effective spectrum.

Since the body transmission is exponential in  $\mathbf{A}$ , we can approximately linearize the measurements by taking logarithms. The results is the log measurement vector

$$\mathbf{L}(\mathbf{A}) = -\log\left(\frac{\mathbf{N}(\mathbf{A})}{\mathbf{N}_0}\right) \quad (5)$$

where  $\mathbf{N}_0$  is the expected value of the measurements with no object in the beam and the division means that corresponding members of the vectors are divided.

Eq. 5 defines a transformation from the log measurements  $\mathbf{L}(\mathbf{A})$  to the A-vector,  $\mathbf{A}$ .

### 2.2 The Invertibility Theorem

The following theorem (Fulks[7] page 284) gives conditions for any two dimension transformation to be invertible:

Let  $F$  be a continuously differentiable mapping defined on an open region  $D$  in  $E^2$ , with range  $R$  in  $E^2$ , and let its Jacobian be never zero in  $D$ . Suppose further that  $C$  is a simple closed curve that, together with its interior (recall the Jordan curve theorem), lies in  $D$ , and that  $F$  is one-to-one on  $C$ . Then the image  $\Gamma$  of  $C$  is a simple closed curve that, together with its interior, lies in  $R$ . Furthermore,  $F$  is one-to-one on the closed region consisting of  $C$  and its interior, so that the inverse transformation can be defined on the closed region consisting of  $\Gamma$  and its interior.

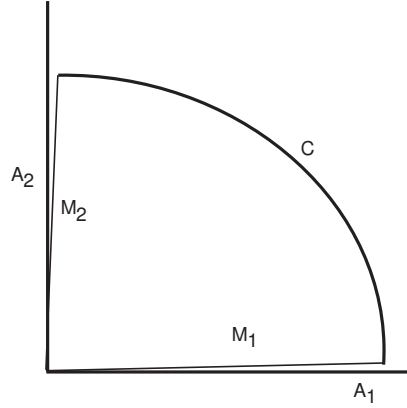


Fig. 1: Closed contour used in proof of invertibility. The contour consists of the two axes, drawn slightly offset here to make them visible, and a quadrant of a circle centered at the origin joining the endpoints of the line segments along the axes.

In Fulks' notation,  $E^2$  is a two dimensional Euclidean space, so this theorem is applicable to the transformation  $\mathbf{L}(\mathbf{A})$  for the two-measurement, two-basis function case.

I paraphrase the theorem as

If the Jacobian of a continuously differentiable two dimensional mapping is nonzero throughout an open region  $D$  and if the mapping is one to one on a simple closed curve  $C$  which lies in  $D$ , then the mapping is one to one and invertible on  $C$  and its interior.

Fulks uses the term "Jacobian" to refer to the determinant of the Jacobian matrix

$$J = \det \begin{bmatrix} \frac{\partial L_i}{\partial A_j} \end{bmatrix}.$$

I will assume that the converse of the theorem is also true. That is, if the Jacobian determinant is zero in a region, then the transformation is not invertible in that region. This is reasonable given the one-dimension case where a zero derivative implies the transformation is not one-to-one in a region around the zero value and is therefore not invertible.

I discussed the application of this theorem to  $\mathbf{L}(\mathbf{A})$  in previous papers[5, 6, 8]. The proofs in these papers used the contour  $C$ , shown in Fig. 1, which consists of the  $A_1$  and  $A_2$  axes and a section of a circle centered on the origin and joining the end points of the segments on the axes. In the previous papers, I proved that  $\mathbf{L}(\mathbf{A})$  is invertible on the  $A_1$  and  $A_2$  axes under very general conditions since objects whose  $\mathbf{A}$ -vectors are on these axes are composed of only one material.

The previous invertibility proofs on the circular portion of  $C$  are not applicable to some of the spectra in this paper. The proof assumes that the maximum energies in the spectra are different but the spectra discussed below have the same three energies but with different weights. The previous argument was that, due to beam hardening, as the radius of the contour becomes larger the transmitted spectrum approaches a peak at the maximum energy. If the maximum energies of the measurement spectra are different, then the transformation will be invertible on the circle. However, if the maximum energies are the same, the transformation becomes non-invertible for large object thicknesses by the No-Linearize theorem (see Section 6.4 of my dissertation[11] and Chapter 44 of my book[12]). However, the transformation may be invertible for moderate thicknesses if we can guarantee that the circular portion of the contour with a smaller radius is in a region where the Jacobian is non-zero.

### 2.3 Interpretation of the M Matrix and its derivative

For our case, the Jacobian matrix is the matrix  $\mathbf{M}$  with coefficients

$$M_{ij} = \frac{\partial L_i}{\partial A_j}. \quad (6)$$

Since  $L_i = -\log\left(\frac{\lambda_i}{\lambda_{i,0}}\right)$ , we can rewrite the elements of  $\mathbf{M}$  as

$$M_{ij} = -\frac{1}{\lambda_i} \frac{\partial \lambda_i}{\partial A_j}. \quad (7)$$

Substituting the expected value of measurements Eq. 4 in this equation

$$M_{ij} = \frac{\int f_j(E) S_i(E) e^{-\mathbf{A} \cdot \mathbf{f}(E)} dE}{\int S_i(E) e^{-\mathbf{A} \cdot \mathbf{f}(E)} dE}. \quad (8)$$

Defining the normalized spectrum

$$\hat{s}_i(E) = \frac{S_i(E) e^{-\mathbf{A} \cdot \mathbf{f}(E)}}{\int S_i(E) e^{-\mathbf{A} \cdot \mathbf{f}(E)} dE}$$

$$M_{ij} = \int f_j(E) \hat{s}_i(E) dE = \langle f_j(E) \rangle_i. \quad (9)$$

That is,  $M_{ij}$  is the effective value of the  $f_j(E)$  basis function in the transmitted measurement spectrum  $S_i(E) e^{-\mathbf{A} \cdot \mathbf{f}(E)}$ .

The derivative of  $M_{ij}$  with respect to each of the  $\mathbf{A}$ -vector components can be computed by differentiating Eq. 8 using the quotient rule

$$\begin{aligned} \frac{\partial M_{ij}}{\partial A_k} &= \frac{-\lambda_i [\int f_j(E) f_k(E) S_i(E) e^{-\mathbf{A} \cdot \mathbf{f}(E)} dE] + [\int f_j(E) S_i(E) e^{-\mathbf{A} \cdot \mathbf{f}(E)} dE] [\int f_k(E) S_i(E) e^{-\mathbf{A} \cdot \mathbf{f}(E)} dE]}{\lambda_i^2} \\ &= - \left[ \langle f_j(E) f_k(E) \rangle_i - \langle f_j(E) \rangle_i \langle f_k(E) \rangle_i \right] \\ &= M_{ij} M_{ik} - \langle f_j(E) f_k(E) \rangle_i. \end{aligned} \quad (10)$$

In this equation,  $\lambda_i$  is given by Eq. 4 and  $\langle \rangle_i$  is defined in Eq. 9.

The effective values of  $\mathbf{M}$  depend on the transmitted spectrum and are, for most spectra, a function of  $\mathbf{A}$ . If the spectra are single delta functions at energy  $E_1$ ,  $E_2$  such as from an isotope source or a synchrotron source, then

$$\langle f_j(E) f_k(E) \rangle_{i, \text{delta function}} = M_{ij} M_{ik} \quad (11)$$

and  $\partial M_{ij} / \partial A_k = 0$ . With single delta function spectra, there is no beam hardening and the  $M_{ij}$  are constants for all values of  $\mathbf{A}$ . Notice that Eq. 10 has the same form as a covariance.

## 2.4 Analytical formula for endpoints of zero determinant line

Since  $\mathbf{M}$  is a  $2 \times 2$  matrix, its determinant is

$$\det(\mathbf{M}) = M_{11} M_{22} - M_{12} M_{21} \quad (12)$$

To apply the inversion theorem, we need to determine whether the determinant is zero in the first quadrant of the  $\mathbf{A}$  plane. The simulations in Sec. 2.6 show that the product terms  $M_{ij} M_{pq}(\mathbf{A})$  are approximately planar and do not intersect if the transformation is invertible. If the transformation is not invertible, the  $M_{11} M_{22}(\mathbf{A})$  and  $M_{12} M_{21}(\mathbf{A})$  surfaces do intersect and the curve of intersection is approximately a straight line. One approach to develop analytical formulas for invertibility is to determine the line by points of zero determinant on the  $A_1$  and  $A_2$  axes. the intersections of the the product terms on the  $A_1$  and  $A_2$  axes. If the determinant is zero in the first quadrant so the system is invertible, both of the intersections will be not physically feasible, that is, the product terms at the intersection are less than or equal to zero.

Using a linear approximation to the determinant along the  $A_k$ ,  $k = 1, 2$  axes

$$\det(\mathbf{M})(A_k) \approx \det(\mathbf{M})(\mathbf{0}) + \left\{ \frac{\partial}{\partial A_k} [M_{11} M_{22}](\mathbf{0}) - \frac{\partial}{\partial A_k} [M_{12} M_{21}](\mathbf{0}) \right\} A_k. \quad (13)$$

Setting the right hand side equal to zero and solving for  $A_k$

$$A_{k,0} = - \frac{\det(\mathbf{M})(\mathbf{0})}{\frac{\partial}{\partial A_k} [M_{11} M_{22}](\mathbf{0}) - \frac{\partial}{\partial A_k} [M_{12} M_{21}](\mathbf{0})}. \quad (14)$$

We can use the product rule to evaluate the derivatives in the denominator

$$\frac{\partial}{\partial A_k} [M_{ij} M_{pq}] = M_{ij} \frac{\partial M_{pq}}{\partial A_k} + M_{pq} \frac{\partial M_{ij}}{\partial A_k} \quad (15)$$

## 2.5 Analytical condition for invertibility

Using a linear approximation, the value of the diagonal product term,  $[M_{11}M_{22}]$ , at  $A_{k,0}$  is

$$[M_{11}M_{22}]_{lin}(A_{k,0}) \approx M_{11}M_{22}(\mathbf{0}) + \frac{\partial}{\partial A_1} [M_{11}M_{22}](\mathbf{0})A_{k,0}. \quad (16)$$

Note that the diagonal and off diagonal product terms are equal at the  $\det(\mathbf{M})=0$  points. In Sec. 2.6, I show numerically that the linear approximation to  $[M_{11}M_{22}]_{lin}(A_{k,0})$  is positive for the non-invertible spectrum and negative for at least one of the  $A_k$  axes for the invertible spectra.

We can derive an analytical formula for  $[M_{11}M_{22}]_{lin}(A_{k,0})$  by substituting  $A_{k,0}$  from Eq. 14 into Eq. 16 and simplifying:

$$[M_{11}M_{22}]_{lin}(A_{k,0}) = \dots \quad (17)$$

$$\frac{M_{11}M_{22}M_{12}M_{21} \left[ \frac{\langle f_2 f_k \rangle_1}{M_{12}} - \frac{\langle f_1 f_k \rangle_1}{M_{11}} + \frac{\langle f_1 f_k \rangle_2}{M_{21}} - \frac{\langle f_2 f_k \rangle_2}{M_{22}} \right]}{\det(\mathbf{M})(\mathbf{0})(M_{1k}+M_{2k})+M_{21}\langle f_2 f_k \rangle_1 - M_{22}\langle f_1 f_k \rangle_1 + M_{12}\langle f_1 f_k \rangle_2 - M_{11}\langle f_2 f_k \rangle_2}$$

The simulations also show that the denominator of Eq. 17 is positive for the three spectra tested. Since we are only interested in whether the product value is negative or zero and the simulations show the denominator is always positive, we need consider the sign of the numerator of Eq. 17

$$Numerator = M_{11}M_{22}M_{12}M_{21} \left[ \frac{\langle f_2 f_k \rangle_1}{M_{12}} - \frac{\langle f_1 f_k \rangle_1}{M_{11}} + \frac{\langle f_1 f_k \rangle_2}{M_{21}} - \frac{\langle f_2 f_k \rangle_2}{M_{22}} \right]. \quad (18)$$

The elements of  $\mathbf{M}$  are effective values of the basis functions and are always positive so the sign is determined by the expression in brackets of Eq. 18.

Notice that for delta function spectra the first and second and the third and fourth terms of the numerator cancel it is equal to zero. Similarly, the denominator is also zero for delta functions so the product term is indeterminate  $\frac{0}{0}$  and the system will be invertible if the Jacobian determinant at zero thickness is not equal to zero.

## 2.6 Simulations of $\det(\mathbf{M}(\mathbf{A}))$

In the following sections, I will study by computer simulation whether the Jacobian determinant is zero inside  $C$  for several spectra: (1) a set that are known to be non-invertible for two specific  $\mathbf{A}$ -vectors, (2) a similar set that are better conditioned, and (3) x-ray tube spectra with different voltages.

### 2.6.1 3 energy non-invertible

Levine[9] described a set of spectra that he found were not one-to-one. In this section, we analyze these spectra using the methods described in the previous sections. Fig. 2 (a) shows a three dimension plot of the diagonal and off-diagonal  $\mathbf{M}$  elements product terms. Since the determinant is  $\det(\mathbf{M}) = M_{11}M_{22} - M_{12}M_{21}$ , it is zero if the surfaces intersect. Each term is plotted as a separate color-coded surface as shown in the legend of the figure. Part (b) of the figure shows the spectra. From the figure, it is clear that the product term surfaces do intersect on approximately a straight line.

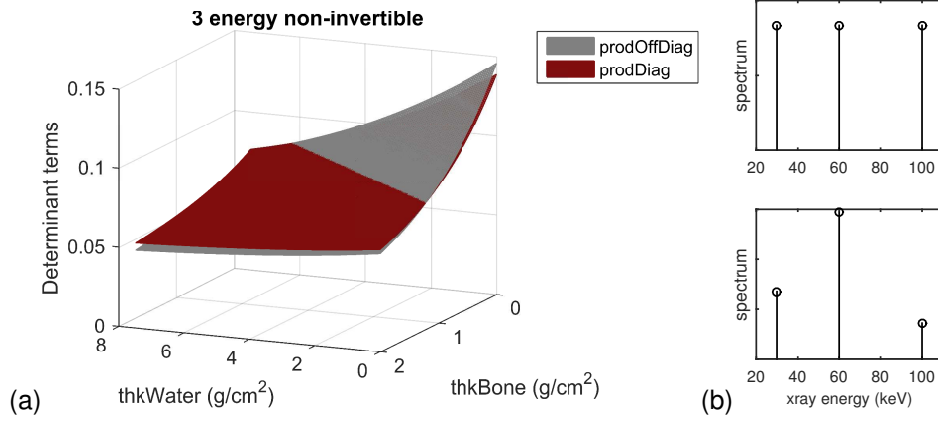


Fig. 2: Three dimension plot (a) of the products of the diagonal and off-diagonal elements of the determinant  $\det(M(\mathbf{A})) = M_{11}M_{22} - M_{12}M_{21}$  as a function of  $\mathbf{A}$  for the Levine non-invertible three energy spectrum. The determinant is zero if the surfaces intersect. Each product term is plotted as a separate color-coded surface as shown in the legend. Part (b) is a plot of the spectra as a function of x-ray energy.

Fig. 3 shows views of the diagonal and off-diagonal  $M$  elements product data projected onto the  $A$ -plane. Part (a) is a view of the diagonal and off-diagonal determinant terms in Fig. 2 projected along the  $Z$ -axis. Part (b) is an image where the grayscale is proportional to  $1/|\det(M(A))|$ . The bright line in the image shows the zero values. A straight line was fit to the line of maxima and is plotted on the image in yellow. The close fit of the straight line shows that the surfaces are close to planes so their intersection is a line.

Fig. 3 also shows the ambiguous  $A$ -vectors found by Levine plotted as the green crosses. Notice that the points do not fall on the line of zero determinant values.

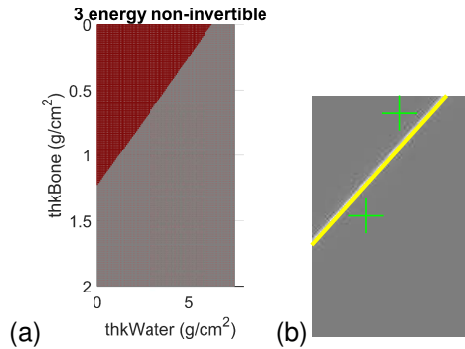


Fig. 3: Projection of the terms of  $\det(M(A))$  onto the  $A$ -plane. Part (a) is a view of the diagonal and off-diagonal determinant terms in Fig. 2 projected along the  $Z$ -axis. Part (b) is an image where the grayscale is proportional to  $1/|\det(M(A))|$ . The bright line in the image shows the zero values. A straight line was fit to the line of maxima and is plotted on the image in yellow. The close fit of the straight line shows that the surfaces are close to planes so their intersection is a line. Also shown is the Levine ambiguous  $A$ -vectors plotted as the green crosses.

Fig. 4 shows one dimensional plots of the diagonal and off-diagonal determinant terms on the  $A_{bone}$  and  $A_{water}$  axes. The curved lines are the actual surfaces with a circle at their intersection where  $\det(M)$  is zero. Also shown are straight line fits to the curved lines using the slope at the origin. The slope was computed with Eq. 15. The intersection of the fit lines is the diamond shape.

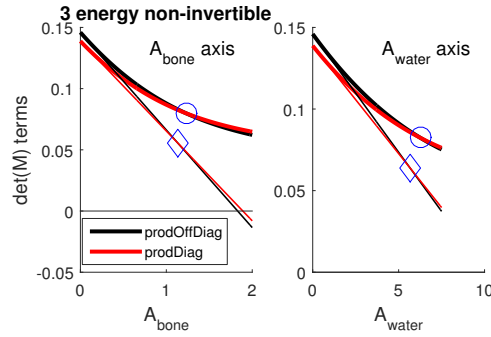


Fig. 4: Plot of the diagonal and off-diagonal surfaces along the  $A_1$  and  $A_2$  axes. The curved lines are the actual surfaces with a circle at their intersection where  $\det(M)$  is zero. Also shown are straight line fits to the curved lines using the slope at the origin. The slope was computed with Eq. 15. The intersection of the fit lines is the diamond shape.

Once the zero determinant points are found on the  $A_k$  axes, we can use them to determine the zero determinant region as the line joining the intersection points. This is the yellow line in part (b) of Fig. 3. The yellow line and the region of large inverse determinant coincide.

### 2.6.2 3 energy invertible

Fig. 5 is a three dimension plot of the products of the diagonal and off-diagonal elements of  $\det(M)$  as a function of  $A$  for well-conditioned three energy spectra. Part (b) is a plot of the spectra. Each product term is plotted as a separate color-coded surface as shown in the legend. Notice that the surfaces do not intersect so the determinant is not equal to zero in the first quadrant of the  $A$ -plane.

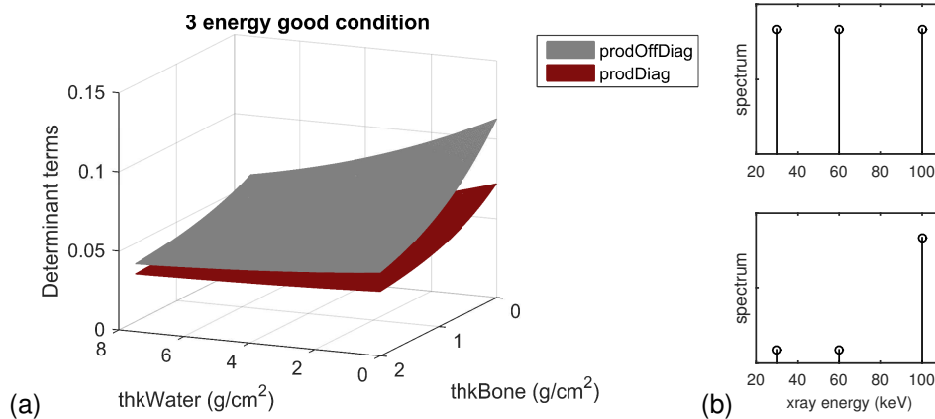


Fig. 5: Three dimension plot of the products of the diagonal and off-diagonal elements of  $\det(M)$  as a function of  $A$  for well-conditioned three energy spectra. Each product term is plotted as a separate color-coded surface as shown in the legend. Notice that the surfaces do not intersect so the determinant is not equal to zero in the first quadrant of the  $A$ -plane. Part (b) is a plot of the spectra.

Fig. 6 shows plots of the diagonal and off-diagonal surfaces along the  $A_1$  and  $A_2$  axes for invertible 3 energy spectra. Notice that the actual product terms, shown by the curved lines, do not intersect. Also shown are the straight lines fit to the derivative at the origin. Their intersection, shown by the diamond icon, occurs outside the region of interest and the product term values are equal to zero, which is mathematically not possible.

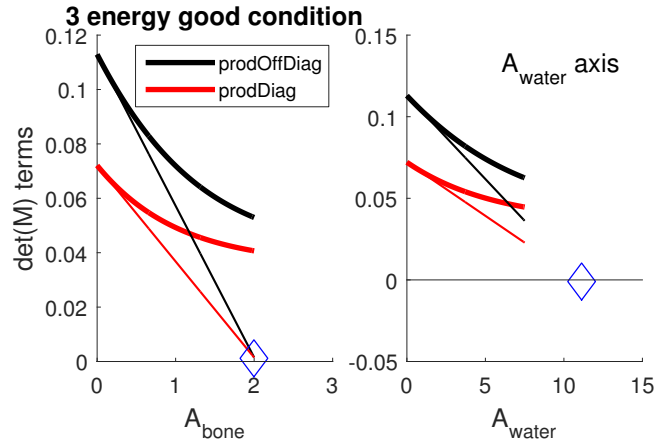


Fig. 6: Plots of the diagonal and off-diagonal surfaces along the  $A_1$  and  $A_2$  axes for invertible 3 energy spectra. Notice that the actual product terms, shown by the curved lines, do not intersect. Also shown are the straight lines fit to the derivative at the origin. Their intersection, shown by the diamond icon, occurs outside the region of interest and the product term values at the intersection are equal to zero, which is physically not possible.

### 2.6.3 Voltage switched x-ray tube spectra

Fig. 7 shows three dimension plot of the diagonal and off-diagonal product terms of  $\det(\mathbf{M})$  for voltage switched (80 and 120 kV) x-ray tube spectra. The surfaces do not intersect so the determinant is not equal to zero.

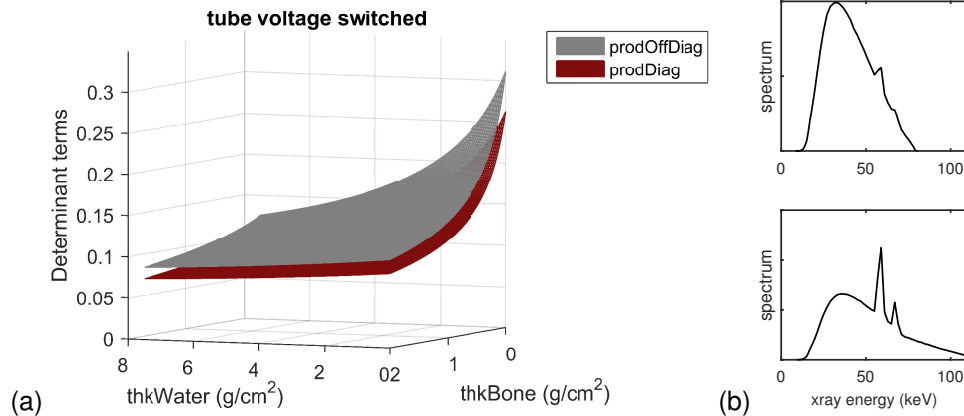


Fig. 7: Three dimension plot of the products of the diagonal and off-diagonal elements of  $\det(\mathbf{M})$  as a function of  $\mathbf{A}$  for voltage switched (80 and 120 kV) x-ray tube spectra. Notice that the surfaces do not intersect so the determinant is not equal to zero in the first quadrant of the  $\mathbf{A}$ -plane. Part (b) is a plot of the spectra. .

Fig. 8 shows plots of the diagonal and off-diagonal surfaces along the  $A_1$  and  $A_2$  axes for the voltage switched spectra. The actual product terms, shown by the curved lines, do not intersect. Also shown are the straight lines fit to the derivative at the origin. At their intersection, shown by the diamond icon, the product term values are negative, which is not physically possible.

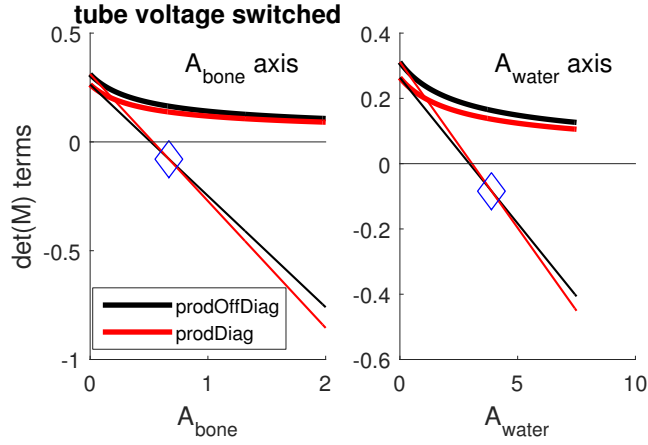


Fig. 8: Plots of the diagonal and off-diagonal surfaces along the  $A_1$  and  $A_2$  axes for the voltage switched spectra. The actual product terms, shown by the curved lines, do not intersect. Also shown are the straight lines fit to the derivative at the origin. At their intersection, shown by the diamond icon, the product term values are negative, which is not physically possible.

### 2.6.4 L data for non-invertible spectra

Fig. 9 shows the  $L$  data for non-invertible 3 energy spectra. Part (a) shows images where the gray scale is proportional to the  $L$  components. The images show the line where the determinant is zero and several lines parallel to it. Part (b) has plots of the  $L$  data on the lines. The values on the central point of the zero determinant line are subtracted for ease of display. Notice that the  $L$  data are not constant on the  $\det(M(A)) = 0$  line.

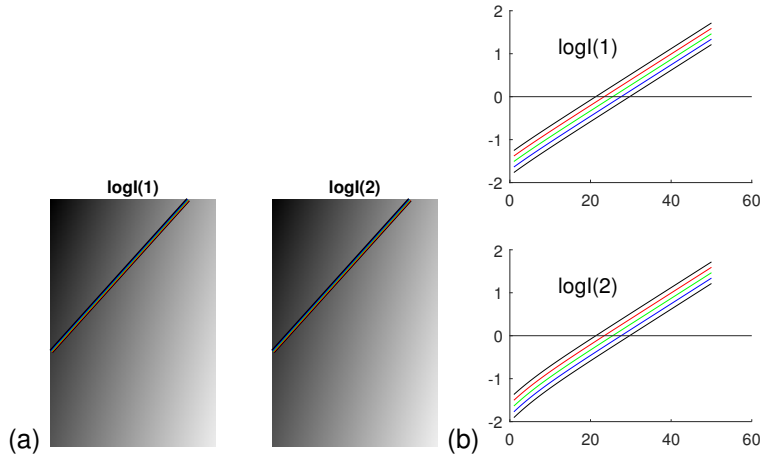


Fig. 9:  $L$  data for non-invertible 3 energy spectra. Part (a) shows images where the gray scale is proportional to the  $L$  components. The images show the line where the determinant is zero and several lines parallel to it. Part (b) has plots of the  $L$  data on the lines. The values on the central point of the zero determinant line are subtracted for ease of display. Notice that the  $L$  data are not constant on the  $\det(M(A)) = 0$  line.

## 2.7 Invert transform with iterative algorithm

The effect of the zero values of the Jacobian determinant on the invertibility of  $L(A)$  was tested with an iterative inverse transform algorithm. The algorithm iteratively found the value of  $A$  that minimized  $|L(A) - L_{input}|^2$ . It was implemented using the Matlab *fminsearch* function.

The norm of the errors of the iterative algorithm for  $A$  values on the green line in Fig. 10(a) were computed. They were plotted as a function of distance along the line in Fig. 10(b). The  $\det(M)$  was zero on the yellow line in Fig. 10(a) and the large errors in Fig. 10(b) are near the point of intersection of the green and yellow lines.

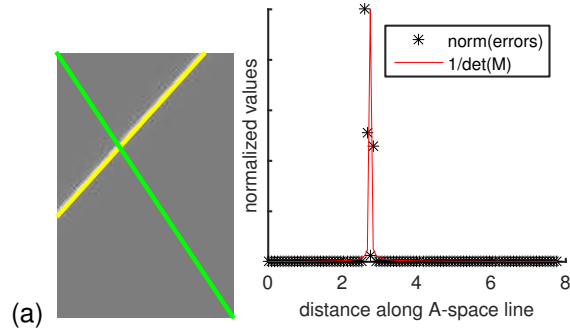


Fig. 10: Effect of  $\det(\mathbf{M}(\mathbf{A}))$  on errors with iterative inverse transform algorithm. The norm of the errors of the iterative algorithm for  $\mathbf{A}$  values on the green line in panel (a) were computed. They were plotted as a function of distance along the line in panel (b). The  $\det(\mathbf{M})$  was zero on the yellow line in panel (a) and the large errors in (b) are near the point of intersection of the green and yellow lines.

### 2.7.1 Iterative algorithm with Levine ambiguous points

The iterative algorithm was also used to test the ambiguous  $\mathbf{A}$  vectors noted by Levine[9],  $[2.5, 1]$  and  $[4.09, 0.13]$ . Using the  $\mathbf{L}$  vector computed for the first  $\mathbf{A}$  as input to the iterative algorithm, the solution depended on the initial point of the iteration. If the point was near one of the two values, the algorithm converged to that value. If the point was far from both, for example the origin, the algorithm converged to  $[2.5, 1]$ .

## 2.8 Values of determinant terms with invertible and non-invertible spectra

As discussed in Sec. 2.5, the analytical formula for signs of values of the product terms at the intersections of the line of zero Jacobian values determines whether the spectra are invertible. The formula was tested with the simulation data described in Sec. 2.6 and the results for the product terms for the three spectra tested are shown in Table 1.

Table 1: Determinant product terms at intersections of zero Jacobian line with  $A_1$  and  $A_2$  axes.

	$A_1$	$A_2$
<b>3 Energy Non-invertible</b>	0.055661	0.063935
<b>3 Energy Good Condition</b>	0.0013775	-0.0011822
<b>Tube Voltage Switched</b>	-0.077947	-0.084209

The theoretical results indicated that the sign of the product terms is determined by the numerator of Eq. 17. Table 2 shows the numerator and denominator of the product terms equation for the tested spectra.

Table 2: Numerator and denominator of Eq. 17 for the product terms of the tested spectra.

Numerator $M_{11}M_{22}$	$A_1$	$A_2$
<b>3 Energy Non-invertible</b>	0.00035307	8.1111e-05
<b>3 Energy Good Condition</b>	2.8091e-05	-4.3262e-06
<b>Tube Voltage Switched</b>	-0.0055665	-0.0010313

Denominator $M_{11}M_{22}$	$A_1$	$A_2$
<b>3 Energy Non-invertible</b>	0.0063432	0.0012686
<b>3 Energy Good Condition</b>	0.020393	0.0036596
<b>Tube Voltage Switched</b>	0.071413	0.012247

## 3 Discussion

The invertibility of spectral measurements is an important issue. Fig. 5 shows that the errors with the iterative algorithm show a sharp increase near the line of non-invertibility. My previous results with a three dimension system [4] showed

that the noise increased by a huge factor near the plane of non-invertibility. X-ray system designers need tools to determine whether their system may become non-invertible in some part of the  $A$ -vector operating range because the system may become unusable near the region of non-invertibility.

In the results shown here, the non-invertible region is nearly a straight line in the two dimension  $A$ -space. In my previous paper[4] the non-invertible region for a three dimension basis set is a plane. The non-invertibility regions for both cases may be explained by the observation that the elements of the  $M$  matrix are nearly linear as a function of  $A$ . The results in Figures 2, 2, and 5 show that the terms in the determinant of  $M$  are also close to linear so their intersection, which results in a zero determinant value, is close to a straight line in two dimensions or a plane in three dimensions.

Sections 2.6 and 2.5 derive analytical formulas for the line of non-invertibility in the two dimension  $A$ -space using a linear approximation to the terms in the determinant of  $M$ . The line is determined by its intersection with the  $A$  axes. For the non-invertible Levine spectrum, Fig. 2.6 shows that the actual and linear approximation intersection points are physically feasible. That is, at positive values and with positive values for the determinant terms at the intersection points. For the invertible three spike spectra, Fig. 2.6 shows that the actual determinant terms do not intersect. The linear approximation does intersect but at the intersection points the determinant product terms are negative which is not physically feasible. For the two voltage x-ray tube spectra, Fig. 2.6 shows that the actual determinant terms again do not intersect and, with the linear approximation, the determinant terms are again negative at the points of intersection.

Table 1 gives the values for the product terms at the intersections with the axes for the three spectra tested. As indicated by the theory, they are positive for the non-invertible spectra and at least one is negative for the three energy good condition and voltage switched spectra, which are both invertible. Table 2 shows that the denominator of Eq. 17 is always positive so the sign of the result for the product term is determined by the numerator and in particular by the expression in brackets in Eq. 18.

Therefore, for the cases tested, the linear approximation gives useful results and the formulas give insight into the conditions leading to non-invertibility. There may, of course, be cases where the linear approximation does not give accurate results. The approach taken was a trade-off between accuracy and simplicity of the formulas. Simple formulas allow us to gain physical insight into the invertibility conditions at the expense of lower accuracy.

Levine[9] introduces an alternate approach to the dual energy inversion problem to that described here. The formulation focuses on the exponent of the transmission equation, Eq. 2. It puts the logarithm of the spectral density in the exponent and combines them with  $A \cdot f(E)$ . The combination is used to derive  $A$ -space surfaces specified by the measurement spectra. The  $A$  vectors that invert the equations are at the intersection of the surfaces. With a particular set of spectra, Levine found two  $A$ -vector points where the surfaces intersect. The transformation is therefore not one-to-one and is not invertible. Interestingly, the two ambiguous points are not on the line of zero determinant.

The results in Fig. 9 show that the  $L$  data on the line of non-invertibility are not constant. Instead, the  $L$  data vary but the two product terms of the determinant balance out resulting in a zero determinant value on this line.

Research is on-going into more accurate theoretical equations for invertibility and ways to apply the formulation described in this paper to clinical systems design.

## 4 Conclusion

An approach to studying the invertibility of spectral measurements is presented and applied to invertible and non-invertible spectra. Non-invertible dual energy spectra have zero Jacobian determinant in the first quadrant of the  $A$  vector plane. For the non-invertible spectra tested, the Jacobian determinant is equal to zero on a curve in the  $A$  vector plane that is close to a straight line. An analytical formula is derived for a linear approximation to the points where the line crosses the  $A$ -axes. If the spectra are invertible, the intersection points are not physically feasible while for the non-invertible spectra they are feasible indicating zero Jacobian determinant values in the first quadrant.

## References

- [1] R. E. Alvarez and A. Macovski, "Energy-selective reconstructions in X-ray computerized tomography," *Phys. Med. Biol.*, vol. 21, pp. 733–44, 1976. [Online]: <http://dx.doi.org/10.1088/0031-9155/21/5/002>
- [2] K. Taguchi and J. S. Iwanczyk, "Vision 20/20: Single photon counting x-ray detectors in medical imaging," *Med. Phys.*, vol. 40, p. 100901, 2013. [Online]: <http://dx.doi.org/10.1118/1.4820371>

- [3] M. Overdick, C. Baumer, K. J. Engel, J. Fink, C. Herrmann, H. Kruger, M. Simon, R. Steadman, and G. Zeitler, "Towards direct conversion detectors for medical imaging with X-rays," *IEEE Trans. Nucl. Sci.*, vol. NSS08, pp. 1527–1535, 2008. [Online]: <http://dx.doi.org/10.1109/NSSMIC.2008.4775117>
- [4] R. Alvarez, "Non-invertibility of spectral x-ray photon counting data with pileup," *arXiv preprint arXiv:1702.04993*, 2017. [Online]: <https://arxiv.org/pdf/1702.04993>
- [5] R. E. Alvarez, "Energy dependent information in x-ray imaging—part 1 the vector space description," *Stanford University Information Systems Laboratory-unpublished*, 1982. [Online]: <http://dx.doi.org/10.13140/RG.2.2.19355.46887>
- [6] L. A. Lehmann and R. E. Alvarez, *Energy Selective Radiography: A Review*. New York: Plenum Press, 1986, pp. 145–187.
- [7] W. Fulks, *Advanced Calculus: An Introduction to Analysis*, 3rd ed. Wiley, 1978.
- [8] R. Alvarez, "Invertibility of spectral x-ray data with pileup—two dimension-two spectrum case," *arXiv preprint arXiv:1703.07557*, 2017. [Online]: <https://arxiv.org/pdf/1703.07557>
- [9] Z. H. Levine, "Nonuniqueness in dual-energy CT," *Med. Phys.*, vol. 44, no. 9, 2017. [Online]: <https://dx.doi.org/10.1002/mp.12298>
- [10] R. E. Alvarez, "Dimensionality and noise in energy selective x-ray imaging," *Med. Phys.*, vol. 40, no. 11, p. 111909, 2013. [Online]: <http://dx.doi.org/10.1118/1.4824057>
- [11] —, "Extraction of Energy Dependent Information in Radiography," Ph.D. dissertation, Stanford University, 1976. [Online]: <http://www.dx.doi.org/10.13140/RG.2.2.12965.09446>
- [12] —, *Topics in Energy-selective X-ray Imaging*, 2017. [Online]: [http://www.researchgate.net/publication/312385192\\_Topics\\_in\\_Energy-selective\\_X-ray\\_Imaging](http://www.researchgate.net/publication/312385192_Topics_in_Energy-selective_X-ray_Imaging)